© 2016. Published by The Company of Biologists Ltd | Journal of Experimental Biology (2016) 219, 1041-1049 doi:10.1242/jeb.132399

RESEARCH ARTICLE

Musculoskeletal modelling of the dragonfly mandible system as an aid to understanding the role of single muscles in an evolutionary context

Sina David[1,*], Johannes Funken[1], Wolfgang Potthast[1,2] and Alexander Blanke[3,*,‡]

ABSTRACT

Insects show a great variety of mouthpart and muscle configurations; however, knowledge of their mouthpart kinematics and muscle activation patterns is fragmentary. Understanding the role of muscle groups during movement and comparing them between insect groups could yield insights into evolutionary patterns and functional constraints. Here, we developed a mathematical inverse dynamic model including distinct muscles for an insect head–mandible–muscle complex based on micro-computed tomography (μCT) data and bite force measurements. With the advent of μCT, it is now possible to obtain precise spatial information about muscle attachment areas and head capsule construction in insects. Our model shows a distinct activation pattern for certain fibre groups potentially related to a geometry-dependent optimization. Muscle activation patterns suggest that intramandibular muscles play a minor role in bite force generation, which is a potential reason for their loss in several lineages of higher insects. Our model is in agreement with previous studies investigating fast and slow muscle fibres and is able to resolve the spatio-temporal activation patterns of these different muscle types in insects. The model used here has a high potential for large-scale comparative analyses on the role of different muscle setups and head capsule designs in the megadiverse insects in order to aid our understanding of insect head capsule and mouthpart evolution under mechanical constraints.

KEY WORDS: Odonata, Insects, Bite force, Inverse dynamics, Muscle activation, Multibody dynamics analysis

INTRODUCTION

Insects originated approximately 480 million years ago (Misof et al., 2014) and developed an astonishing diversity of mouthpart and head capsule types during this time span (Grimaldi and Engel, 2005). From a biomechanical point of view, insect mouthparts are a construction optimized during an extremely long time frame with selection processes leading to an adaptation of mouthparts to changing ecological niches. However, the reasons for the absence or presence of certain mouthpart muscles are still unclear. Functional requirements related to food uptake are a potential cause, but the amount of 'functional influence' on the evolution of mouthpart musculature is difficult to determine (Spagna et al., 2008), although these muscles are used as characters for phylogenetic reconstruction (e.g. Staniczek, 2000). In this context, an analysis of insect mouthpart and muscle kinematics can provide a useful toolbox to assess the role of a given muscle equipment and compare it with other species in an evolutionary context.

Dragonflies (Odonata) are an interesting case in this regard. They possess a suite of six to seven mandibular muscles, thus showing a plesiomorphic muscle equipment with respect to all other winged insects except mayflies (Ephemeroptera), which possess eight (Staniczek, 2000). However, regarding their mandible joints and the configuration of the mandibular teeth (or incisivi), Odonata show the typical ball-and-socket joints and incisivi of many 'higher' insects (Neoptera; Blanke et al., 2012; Staniczek, 2000, 2001; Wipfler et al., 2011). In particular, the mandibular system (joint types, muscles, mandible motion) of Odonata, Ephemeroptera and Neoptera has been intensely studied concerning its phylogenetic value to infer the relationships of these three groups to each other (Staniczek, 2000, 2001). Two hypotheses, Metapterygota (Odonata+Neoptera) and Palaeoptera (Odonata+Ephemeroptera) are currently mainly discussed (Beutel and Gorb, 2006; Blanke et al., 2012, 2013a; Brauckmann and Zessin, 1989; Misof et al., 2014; Ogden and Whiting, 2003; Pass, 2000, 2006; Staniczek, 2000; Terry and Whiting, 2005; Wheeler et al., 2001; Willkommen and Hörnschemeyer, 2007).

There is fragmentary knowledge of the mouthpart kinematics for a few insect species, mostly within certain ant subfamilies (Gronenberg, 1995; Gronenberg et al., 1997; Spagna et al., 2008) or beetles (Evans, 1964; Forsythe, 1982, 1983). Most of these studies provide external investigations on the movement of single mouthparts during food uptake without information on the role of related muscles and muscle actions (Evans, 1964; Forsythe, 1982, 1983; Popham, 1959). A notable exception is the investigation of Schmitt et al. (2014), who used high-speed micro-computed tomography (μCT) to investigate the coordination of mandibles, maxillae and the labium during biting, but without primary data on mandible muscle geometry and activation during the biting cycle. However, there is to our knowledge no direct method to accurately study muscle activation patterns (MAPs) and muscle movement on a micrometre scale necessary for insects mouthparts (Julian, 1969).

Inverse dynamic models, including distinct muscles, would allow for indirect calculation to predict muscle forces and activation. To determine the resulting internal forces and moments of force, the models need as input parameters the individual geometry and kinematics of the considered segments (e.g. mandibles and head capsule) as well as the external forces (e.g. total bite force) and moments. Furthermore, by use of optimization procedures, muscle-specific force–length, force–velocity and force–activation relationships, muscle forces and muscle activations can be determined (Zatsiorsky, 2002). Such inverse dynamic models are becoming increasingly popular under the umbrella term 'multibody

[1]Institute of Biomechanics and Orthopaedics, German Sport University Cologne, Cologne 50933, Germany. [2]ARCUS Clinics Pforzheim, Rastatter Strasse 17-19, Pforzheim 75179, Germany. [3]Medical and Biological Engineering Research Group, School of Engineering, University of Hull, Hull HU6 7RX, UK.
*These authors contributed equally to this work

‡Author for correspondence (a.blanke@hull.ac.uk)

Received 9 December 2015; Accepted 25 January 2016

Journal of Experimental Biology (2016) 219, 1041-1049 doi:10.1242/jeb.132399

dynamics analysis' (MDA). MDA has been used to determine muscle activations and forces, joint reaction forces and mouthpart movement parameters in a range of extant (Curtis et al., 2010a; Gröning et al., 2013; Moazen et al., 2008) and extinct vertebrates (Bates and Falkingham, 2012), as well as in human movement analysis (e.g. Pandy, 2001). The prediction of muscle activation and bite force through MDA has been validated (Curtis et al., 2010b), but at the same time models are extremely sensitive to muscle geometry (Gröning et al., 2013).

Here, we developed and tested an MDA model based on µCT and bite force measurements. As an example, we analysed the muscle kinematics of a dragonfly by segmenting the CT data at the voxel level. We subsequently investigated the role of the mandibular muscles during biting in this dragonfly by using musculoskeletal modelling software that has been validated for vertebrate movement research (Curtis et al., 2010a,b; Watson et al., 2014; Wehner et al., 2010). Bite force measurements provide the basis for the modelling of MAPs and the change of muscle geometries during biting. The proposed workflow has wider applications, as it generally allows for the prediction of MAPs in small animals with extremely small moving parts, principally only restricted by the resolution of the available µCT data, which influences the accuracy of the geometry of the resulting muscle model.

MATERIALS AND METHODS

Bite force measurements

Five living *Sympetrum vulgatum* (Linnaeus 1758) males (Anisoptera: Libellulidae) were used for our measurements. The mouthparts of Odonata are directed ventrally (orthognathous) and the space between the outermost incisivi of the mandibles is species dependent in the range of 2–7 mm when fully abducted (Movie 1). In order to measure the bite force in the narrow space between the mandibular incisivi, a piezoelectric mini force sensor (SKB pin-force sensor Z18152X2A3sp, Kistler, Winterthur, Switzerland) of 0.60 mm thickness was used. The active surface zone of the sensor spans an area of 4×1.5 mm. The effective range of the sensor is 0–5 N with a sensitivity of 6 pC N^{-1} (noise <0.01 Npp, where Npp is the peak to peak noise; linearity error <5%). The sensor signal was amplified using a charge amplifier (Charge Meter Type 5015, Kistler). Analog data were analog–digital converted (MX Ultranet HD, Vicon, Oxford, UK) and recorded with a frequency of 1000 Hz.

Dragonflies were fixed at the thorax with a custom-built fixation device consisting of a flexible cushioned plastic calliper on a metal base unit (Fig. 1A,B). The calliper strength was adjustable, allowing for optimal fixation of the dragonfly. The force sensor was similarly fixed with a calliper on a metal base unit. Both units were adjustable in the horizontal and vertical plane so that the sensor could be moved inside the oral opening of the specimen (Fig. 1B).

The natural reflex of captured dragonflies is to bite at objects between the mandibles, which meant that measurements could be taken immediately. The sensor was positioned between the mouthparts (Movie 1) and bites were recorded for 30–59 s, depending on the dragonflies' biting behaviour. In total, six bite series were captured. The longest bite series was chosen for further analysis. It was subsequently filtered (Butterworth, low pass, fourth order, 50 Hz cut-off, recursive) and the 10 strongest single bites were extracted and used for the inverse dynamic calculations. Single bites were selected, when the force–time curve showed a continuous increase of at least 0.02 N, an unambiguously identifiable absolute maximum, the absence of local minima between biting onset and peak force and the absence of movement artifacts due to movement of the insect (as visible, for example, between 0 and 2 s in Fig. 2A).

Kinematic muscle model setup

In order to build a geometrically precise kinematic muscle model of the dragonfly's head, we scanned one specimen using high-resolution synchrotron radiation µCT (SR-µCT) (Betz et al., 2007). The live specimen was put into Bouin solution (Romeis, 1989), stored for 3 days to allow full penetration of the fixative and subsequently washed in 70% ethanol. In order to avoid shrinking artifacts of the internal anatomy as much as possible, the sample was

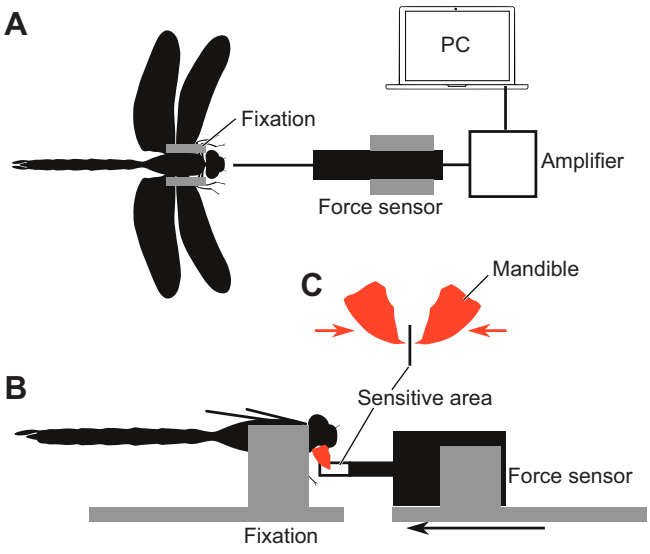

Fig. 1. Experimental setup for bite force measurements. (A) Dorsal view. (B) Lateral view. (C) Detail of the mandibles biting on the sensitive area.

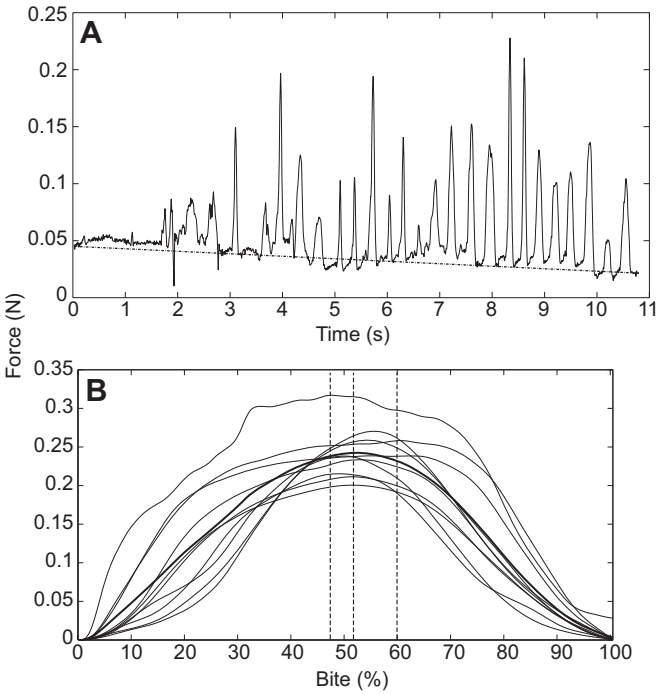

Fig. 2. Bite force. (A) Example bite force curves during 10 s of measurement (total measurement time, ~59 s) in one specimen of *S. vulgatum*. The signal was bandpass filtered (0.1, 50 Hz). The dotted line indicates sensor drift. (B) The 10 strongest bites measured. Dotted lines show the mean±s.d. interval when maximum bite force is reached. Refer to Fig. S1 for raw data.

Journal of Experimental Biology

Journal of Experimental Biology (2016) 219, 1041-1049 doi:10.1242/jeb.132399

critical point dried (Model E4850, Bio-Rad) and afterwards mounted on beamline-specific specimen holders. SR-µCT was done at the Deutsches Elektronen Synchrotron (DESY, Hamburg, Germany), beamline DORIS III/BW2 at 8 keV in absorption contrast mode (Beckmann et al., 2008) with 2.7× magnification and a voxel size of 5 µm (isotropic). Additionally, specimens in 70% ethanol were manually dissected to observe the muscle attachments under natural conditions.

Model creation

Subsequent segmentation of the reconstructed image stacks was accomplished with the open-source program ITK-SNAP (Yushkevich et al., 2006) (GPL licence; www.itksnap.org/pmwiki/pmwiki.php). We used the 'region competition' segmentation algorithm based on grey value differences for semi-automatic 3D segmentation. Because of the superior image data generated from the SR-µCT setup at DESY beamline BW2, grey values within the image data were tissue dependent, allowing for a clear discrimination of muscle, chitin and nervous tissue. ITK-SNAP allows for voxel-level segmentation of the image data; therefore, the precision of the resulting 3D objects is only limited by the voxel size of the underlying SR-µCT dataset (5 µm isotropic in our case). In order to analyse the muscle activation patterns, we segmented the head, mandibles and origin and insertion of the mandibular muscles (Fig. 3A).

Segmentations were exported in Standard Tessellation Language (STL) format and imported into Blender™ (GPL licence; www.blender.org). Origin and insertion fields of muscles were connected by joining the respective objects. Muscle representations were then exported as object files (OBJ) and imported into the AnyBody Modeling System™ (http://www.anybodytech.com/; Fig. 3B). Mandibles and the head were exported as STL files in ASCII syntax for import into the AnyBody Modeling System™. By choosing 'Forward –Z' and 'Up Y' in Blender, the export of both OBJ and STL files within the same coordinate reference system and with the same coordinate directions was ensured. The force sensor was modelled as a force plate between the mandibles in Blender and exported as an STL file for import into the AnyBody Modeling System™.

Head segments

In the AnyBody Modeling System™, the segment coordinate systems of the imported head and mandible objects were attached to the respective centre of mass. The head capsule was furthermore linked to the environment coordinate system (global coordinate system). The segmentation data were used for surface definition, location of the segment's centre of mass and moments of inertia of each segment. The segment masses were measured with a Sartorius 1712 scale (Sartorius GMBH, Goettingen, Germany).

Mandible joints

The model contains four spherical joints, an anterior and posterior one on each mandible (ama and pma; Fig. 3C,D). The rotation centre of each joint was assumed to be the middle of the spherical joint. The two joints of each mandible create a virtual revolute joint with an axis aligning the two spherical joints (Fig. 3C,D). This eliminates five of the originally six rotational degrees of freedom (three in each joint). In order to align the single rotation centres of the joints, we rotated the coordinate systems of each joint. A rotation matrix was generated, with the origin lying in the middle of the two joints, pointing with Y in the direction of joint pma (u). The second axis (v) was defined as perpendicular to u and pointing to the tip of the mandible; the third axis was defined as perpendicular to u and v (Fig. 3D).

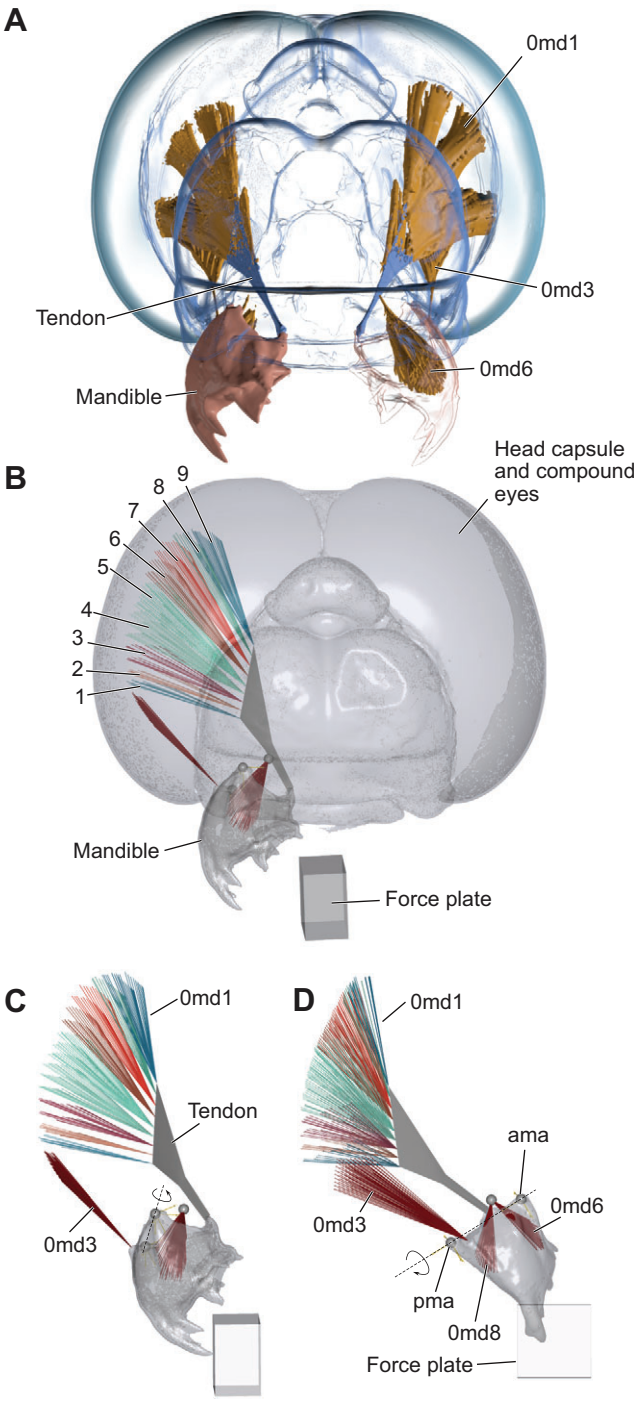

Fig. 3. Model creation. (A) 3D reconstruction of the mandibular muscle equipment of *Sympetrum vulgatum*. Muscles (orange) show shrinkage artifacts due to sample preparation for synchrotron radiation-micro-computed tomography (SR-µCT). Compound eyes, turquoise (semitransparent); head, blue (semitransparent); mandibles, red (semitransparent); tendons, light blue. (B) AnyBody Modeling System™ model of *S. vulgatum* showing the mandibular muscle setup for the right side and defined muscle groups of 0md1. Muscle group numbers correspond to the numbers used in Fig. 5. (C) Detail of B. (D) Lateral view of the mandible muscle locations. 0md5 is not shown, as it is mostly covered by 0md6. The dotted line indicates the axis of rotation. ama, anterior mandibular articulation; pma, posterior mandibular articulation; 0md1, m. craniomandibularis internus; 0md3, m. craniomandibularis externus posterior; 0md5, m. tentoriomandibularis lateralis superior; 0md6, m. tentoriomandibularis lateralis inferior; 0md8, m. tentoriomandibularis medialis inferior.

Constraints

The range of motion of the virtual revolute joints was extracted from the video footage of the biting sequences (Movie 1).

Muscles

To attach the muscles to the segments, we defined segment nodes accounting for the origin or insertion of each muscle according to the segmentation data, thus linking the head segments with precise muscle origins and insertions (Fig. 3C). As most muscles cover a wide area of origin, we defined numerous single muscles in order to account for the pennation of a given muscle bundle.

The origin and insertion nodes were connected with 'viapoint' muscles in the AnyBody Modeling System™, which means that the muscle length is simulated as the shortest distance between the origin and insertion point of a given muscle in a non-static condition. This is in agreement with the geometric muscle relationships based on morphological data of dragonflies (Fig. 3A) (Blanke et al., 2013b,c).

Muscle model

Muscles react to activation signals by changing their geometry, which produces force as an output (Hill, 1938; Thelen, 2003; Zajac, 1989). In inverse dynamics as used here, the measured external force is the input and the force generated by the muscle as well as the activation of the muscle are the outputs. Thus, the model is mathematically reversed (Zatsiorsky, 2002). The AnyBody Modeling System™ provides three different types of muscle models ('AnySimpleMuscleModel', 'AnyMuscleModel2EL' and 'AnyMuscleModel3EL'). We modelled all muscles according to the simple muscle model, which contains one element and assumes a constant strength of the muscle. This muscle model requires only the definition of the initial muscle force; the rest of the parameters are modelled according to the assumptions of the Hill-type model (Hill, 1938; Zajac, 1989). Previous studies found good agreement between the simple muscle model and more parameter-intensive models when slower movements are simulated (Damsgaard et al., 2006; Duprey et al., 2015). The simple muscle model basically ignores the differing behaviour of non-contractile elements (e.g. tendons) and contractile elements (e.g. actin and myosin). Because factors like initial muscle force, contraction velocity and length of the non-contractile elements are unknown for dragonfly head muscles, the usage of the simple muscle model is currently the best working hypothesis (Zajac, 1989).

Muscle simulation

In the reverse direction approach, the initial muscle force was obtained by assuming that the testing situation simulates a life-threatening situation for the dragonfly (as the thorax is pressed by the fixation device). We thus hypothesized that the bite cycle is carried out with maximum neuronal stimulation.

This assumption affects the choice of the muscle recruitment criterion, which is the basis for determining which set of muscle forces will balance the external bite load (Damsgaard et al., 2006). The AnyBody Modeling System™ software allows the choice between several recruitment criteria. A linear criterion recruits a minimum number of muscles to balance the system. This is a non-physiological approach (Damsgaard et al., 2006) and therefore was not used here. The minimum/maximum criterion models the sum of all muscle activation levels as low as possible, i.e. with the lowest possible energy cost (Damsgaard et al., 2006; Rasmussen et al., 2001). This criterion is realistic when fatigue and maximal cost efficiency play a role in muscle activation (Damsgaard et al., 2006). Because it was shown that muscle activation-minimizing strategies (economic muscle activation) have not been found in animals yet (Hubel and Usherwood, 2015) and the dragonfly was able to continue biting over a period of 59 s with some of the highest bite forces measured during the end of the measurement cycle, the minimum/maximum criterion was not considered realistic.

The quadratic muscle criterion as used here optimizes fibre recruitment by evenly distributing activation across all involved fibres of the muscle, but also taking into account the geometric position of each fibre. Thus, fibres with an advantageous location are preferred for activation until other factors like force–length or force–velocity ratios are more advantageous for other fibres within the muscle. This criterion additionally agrees well with electromyographic (EMG) data, and measured muscle and joint reaction forces (Crowninshield and Brand, 1981; Siemienski, 1992). Because the dragonfly was able to continue biting over a longer period with some of the highest bite forces measured during the end of the measurement cycle, a maximum muscle activation of 80% was hypothesized. Starting from 0.4 N, which was obtained in previous studies on insect muscle (Blümel et al., 2012a), the inverse dynamics analysis recorded muscle activation well below 80% [probably since Blümel et al. (2012a) investigated a whole muscle instead of single fibres]. Therefore, the initial force of the muscle was lowered until a maximum muscle activation of 80% was reached during the strongest bite cycle. This approach leads to an initial force for each muscle fibre of 0.0029 N.

Tendons

Although frequently termed 'tendon', these structures in insects are partly heavily sclerotized (Paul and Gronenberg, 1999). As we follow the terminology of Beutel et al. (2013) and Wipfler et al. (2011), and to allow for comparison with the literature record, we retained the term 'tendon' here. Because of this sclerotization, the material properties of this structure cannot be compared with tendon-like structures in, for example, vertebrates. Previous analyses in vertebrates revealed tendon to be very stiff in material behaviour (Kubo et al., 1999); thus, we modelled the large tendon of M. craniomandibularis internus as a rigid segment (Fig. 3). The tendon of the M. craniomandibularis internus is of flat, triangular form, inserting dorsal of the incisivi at the proximolateral ridge of the mandible.

For analysis of muscle activities during biting, we first studied the kinematics and inverse dynamics of the whole natural muscle set. In order to explore the role of single muscles or functional muscle groups, we ran separate analyses (artificial biting scenarios) with only the large mandibular adductor as the active muscle as well as analyses with only the smaller intramandibular muscles as active muscles (see below for an explanation of mandible muscle configuration).

RESULTS

Dragonfly mandible movement and bite force

Dragonflies possess an anterior and a posterior fixed ball-and-socket joint on each mandible (ama and pma; Fig. 3C,D). Thus, a virtual revolute joint is present between the two joints, which limits mandible motion to a rotation in the transversal plane around that virtual revolute joint (Fig. 3C). The mandible muscle system of *S. vulgatum* is composed of five muscles – one abductor (M. craniomandibularis externus posterior; 0md3) and four adductors (M. craniomandibularis internus, 0md1; M. tentoriomandibularis lateralis superior, 0md5; M. tentoriomandibularis lateralis inferior,

Journal of Experimental Biology (2016) 219, 1041-1049 doi:10.1242/jeb.132399

0md6; M. tentoriomandibularis medialis inferior, 0md8) – which are responsible for movement of the mandible (Fig. 3). While 0md1 +3 originate at the head capsule (Fig. 3A), 0md5+6+8 (hereafter 0md5–8) all originate at the tentorium – an endoskeletal structure within the head of insects (Fig. 3C,D).

Time-normalized (0%: start of sensor contact; 100%: end of sensor contact) bite curves are bell shaped, with peak bite forces reached at 52.3±3.7% of the bite (Fig. 2B) and a steep increase of bite force during the first 30% of the contact phase. The earliest maximum was reached at 47.5%, the latest at 60.5%. Average bite duration was 197.5±51.3 ms (Fig. 2A). Maximum measured bite force was 0.31 N; mean peak bite force over the 10 strongest bites was 0.244±0.034 N. Bite force then rapidly decreased after 70% of the contact phase (Fig. 2B). During the strongest bites (Fig. 2B; Fig. S1), a short exponential increase of bite force was recorded from ca. 70% of the bite followed by a plateau-like progression towards maximum activation level.

Muscle activation during biting

In the following we will focus on the strongest measured bite cycle (SB=0.31 N), an intermediate bite cycle (IB=0.27 N) and the weakest bite cycle (WB=0.2 N) out of the 10 strongest measured bite cycles (0%: start of sensor contact, 100%: peak bite force). Percentage activation will be described in the following order: SB%/IB%/WB%. Percentage muscle activation for 0md1 is given as the mean of the maximum activation of each fibre group. Activation for 0md5–8 is given as the maximum activation of each fibre. For all muscles, activation was normalized against the respective maximum force modelled for each muscle fibre.

Generally, muscle activation of the mandible abductor 0md3 was characterized by a steep decrease of activation (Fig. S1). 0md3 activation remained at zero through the rest of the biting process. At the beginning of the contact with the force plate, the first activation was recorded for the main mandibular adductor 0md1, followed shortly after by 0md5–8 (Fig. 4A–C). 0md1 activities reached 40%/28%/28% of total potential muscle activation. After this first peak, all muscles showed a drop off in activation of ∼12% (SB) to over 20% (IB) and 17% (WB). Note that intermediate drop off in activation was higher in the IB scenario. Activation then gradually increased in the SB scenario while IB and WB showed a partly exponential increase followed by an asymptotic curve progression towards maximal muscle activation at 62%/52%/40%. Muscle fibre groups of 0md1 showed nearly 12%/15%/12% spread in activation (Fig. 4). The smaller muscles 0md5–8 showed percentage activation differences of 10%/8%/7% for 0md6+8 and 4%/4%/2% for 0md5.

Artificial biting scenarios

Simulation of biting only with 0md1 activated resulted in an activation increase of 0md1 by 7%|7%|25% for the investigated bites (Fig. 4D–F). Without 0md1 but with muscles 0md5–8 active, the initial force of these muscles had to be increased fivefold to 0.014 N. Activation of these three muscles increased by ∼230%/230%/230% in order to execute the same bite force at the tips of the mandibles (Fig. 4D–F). Fibre activation spread was greater than in the natural muscle setup (Fig. 4A–C).

Spatial muscle activation during biting

The single fibre groups of 0md1 showed a differing activation spread from each other and between the SB, IB and WB scenarios (Fig. 5). Within a fibre group, activation spread was widest in those groups that showed the highest activation (Fig. 5C–G). An exception is fibre group 9 which showed a 45% activation spread

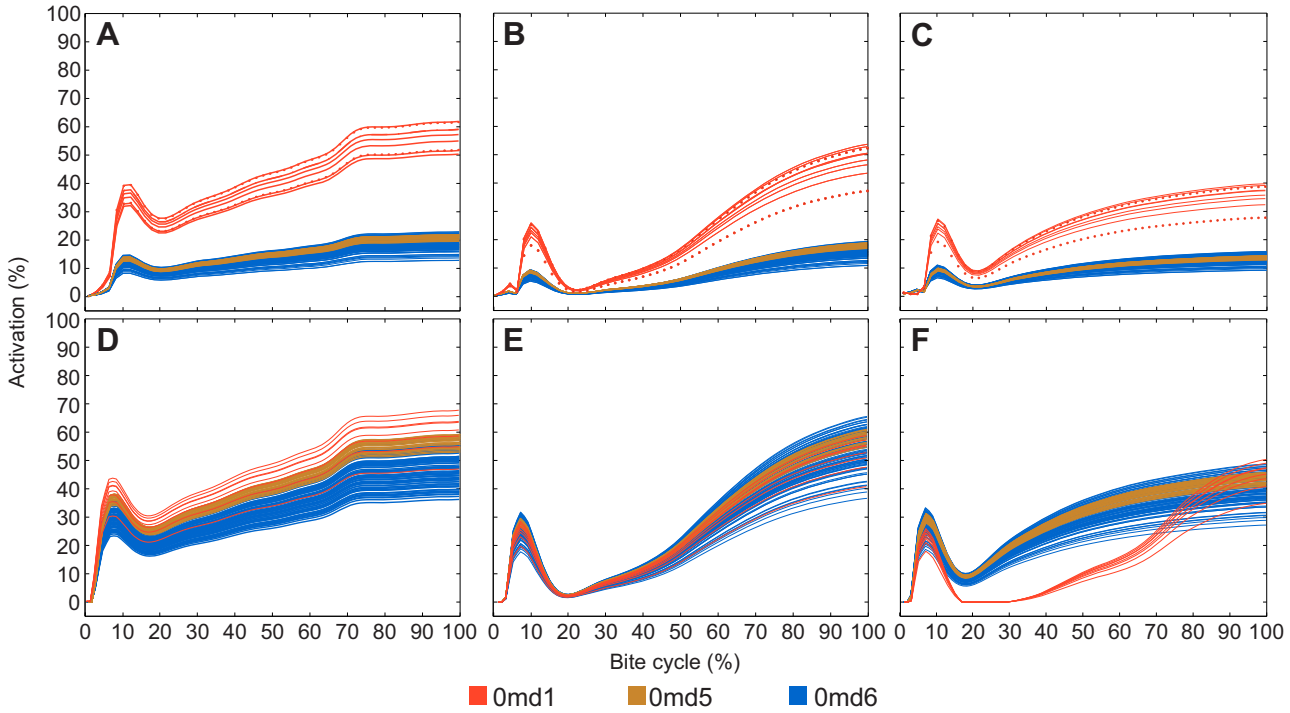

Fig. 4. Muscle activation during biting. (A–C) Muscle activation during the strongest measured bite cycle (SB; A), an intermediate bite cycle (IB; B) and the weakest bite cycle (WB; C) out of the 10 strongest bite cycles measured in one animal. (D–F) Muscle activation for the artificial biting scenarios: 0md1 activation without activation of other muscles; 0md5+6 activation without activation of 0md1. (D) SB, (E) IB and (F) WB. Activation patterns are shown for each muscle fibre (or group of fibres in the case of 0md1). Muscle 0md8 is not shown as its activation patterns overlap with those of muscle 0md6. Activation was normalized against the maximum force modelled for each muscle fibre; bite duration was normalized against contact time.

Journal of Experimental Biology

Journal of Experimental Biology (2016) 219, 1041-1049 doi:10.1242/jeb.132399

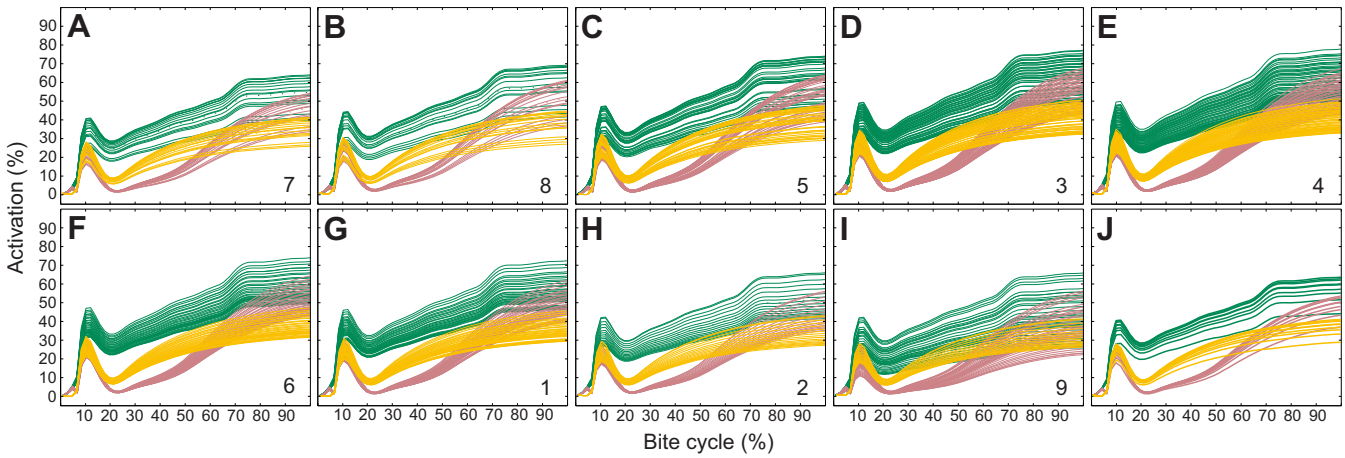

Fig. 5. Spatial muscle activation during biting. (A–I) Activation patterns (activation spread within a given fibre group) for each of the defined fibre groups of 0md1 during biting for the strongest bite (green), an intermediate bite (red) and the weakest bite (yellow) of the 10 strongest bites analysed in one animal. Numbers (bottom right) correspond to muscle groups shown in Fig. 3. (J) Mean activation patterns of each fibre group. Activation was normalized against the maximum force modelled for each fibre; bite duration was normalized against contact time.

(Fig. 5I) comparable to that of the fibre groups with higher overall activation. During intermediate biting, the activation in all fibre groups was distinctly lower than the activation for the weakest bite cycle at 20–50% of the bite time. Muscle activation spread conformed with bite strength, where intermediate biting showed a greater spread than that for the weakest bite cycle.

The single fibre groups of 0md1 also showed a distinctive spatial activation pattern (Fig. 6). Highest activation was recorded for those fibres attached in the middle portion of the tendon, whereas the fibre groups inserting dorsally and ventrally at the tendon showed the lowest overall activation.

DISCUSSION

The bite cycle characteristic for *S. vulgatum* shows a stereotypical pattern with approximately 3 bite cycles s^{-1} and overall similar bite curve geometries (Fig. 2A; Fig. S1). This suggests a highly stereotypical neuronal control pattern, which is in agreement with previous studies for cockroaches (Schmitt et al., 2014) and the locust (Blaney and Chapman, 1970). In contrast, bite cycles are shorter than in cockroaches and the locust (Blaney and Chapman, 1970; Schmitt et al., 2014). Measured bite force for *S. vulgatum* is in the range of bite force results for cockroaches (Weihmann et al., 2015) or stag beetles (*Cyclommatus metallifer*) (Goyens et al., 2014; Wheater and Evans, 1989). Successive bite cycles typically lasted between 30 and 59 s with some of the strongest bite cycles occurring during the end of the measurements (Fig. S1). Given the duration of the bite cycles, fatigue may not play a role in the biting process, which would in turn suggest that the muscles are neuronally probably not stimulated to their respective maximum force outputs even when the specimen is heavily stressed. Again, this points towards a stereotypical neuronal control pattern for the biting process, which is in agreement with studies investigating, for example, insect leg movement (Bässler, 1988; Büschges et al., 2008). In this context, non optimal pre-stretching and resting lengths of the muscles could be another factor influencing maximum force output. Under isometric conditions, it was shown that pre-stretching effects account for ∼1% of the total muscle output (Blümel et al., 2012a) and affect total muscle output during the first 0.1–0.5 s. Although we have to assume concentric loading conditions in our case, muscle activity modelling was done only for the time steps after contact with the force plate. We therefore hypothesize that non-optimal pre-stretching is negligible for the time frames we measured but has to be accounted for where initial muscle activation during the beginning of a given movement is modelled.

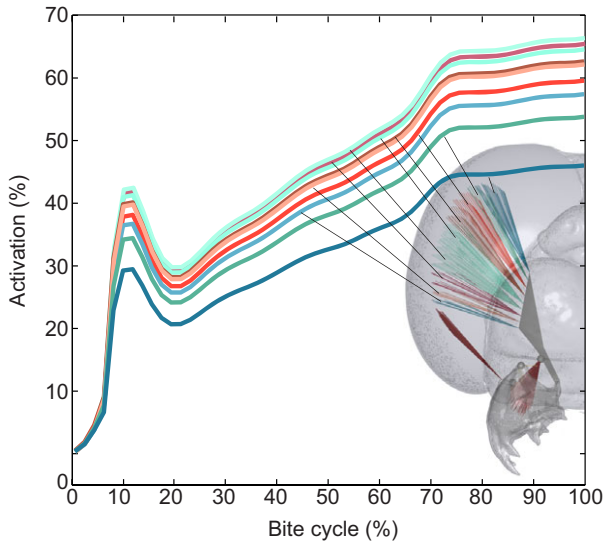

Fig. 6. Mean activation patterns for each of the defined fibre groups of 0md1 for the strongest bite cycle according to fibre location. Activation was normalized against the respective maximum force of each fibre.

Muscle activation patterns showed that muscle 0md1 acts as the main adductor under all biting scenarios. This was to be expected given that 0md1 is by far the largest muscle in the dragonfly head (Beutel et al., 2013; von Kéler, 1963). During the strongest bite cycle analysed (Figs 2B, 4A), we could also record the characteristic additional activation of the so-called 'slower muscle fibres' already reported in, for example, ants (Paul and Gronenberg, 1999), which can produce higher forces at slower activation speeds (Paul and Gronenberg, 2002). The temporal activation pattern simulated by the AnyBody Modeling System™ model thus corresponds to earlier *in vivo* measurements of muscle neuronal control and activation (Paul and Gronenberg, 2002). The conspicuous pattern of the strongest recorded bite cycles shows that our simulation can account for slight variations in bite geometry and model muscle activation patterns accordingly. A higher recording frequency (1000 Hz in our

case) may be advantageous in order to resolve bite force variations within a single bite cycle compared with previous studies (Goyens et al., 2014; Weihmann et al., 2015).

With the musculoskeletal model developed here, the role of the other smaller mandibular adductors 0md5–8 during biting could be assessed. Data for intermediate and weak bites show that during the initial bite phase the intramandibular muscles 0md5–8 account for nearly 50% (IB) or 30% (WB) of the total activation, while during later parts of the bite cycle the activation increase is much lower than for 0md1 (Fig. 4B,C).

Given these results, it can be expected that 0md5–8 do not play a significant role during biting in dicondylic insects, while their input in more basal insects with loose mandibular joints such as Zygentoma (silverfish) and Archaeognatha (jumping bristletails) may be more significant. Indeed, our artificial setup with only 0md5–8 present as adductors (Fig. 4D–F) resulted in muscle overload if the same initial force was assumed. The initial force of each muscle fibre therefore had to be increased fivefold in order to generate the same bite force. These results correspond to the configuration of these muscles in more 'basal' insects like silverfish, bristletails and even two-pronged bristletails: in these groups, 0md5–8 have a larger volume, 0md6+8 nearly fill out the lumen of the mandibles completely, while 0md1 is comparably smaller (Bitsch, 1963; Blanke et al., 2014, 2015; Staniczek, 2000). In many 'higher' insects such as certain Grylloblattodea, Mantodea and Orthoptera, a part or all of muscles 0md5–8 are absent (Blanke et al., 2012). We therefore suggest that muscles 0md5–8 do not play a crucial role during biting in winged insects like Ephemeroptera, Odonata and Polyneoptera and accordingly were reduced in some higher lineages of insects [see character matrices in, for example, Blanke et al. (2012, 2013a,c) and Wipfler et al. (2011) for presence/absence of these muscles within winged insect orders].

The spatial activation of the fibre groups within 0md1 (Figs 5, 6) shows a distinct pattern according to the origin and insertion of each fibre group. Fibre groups 1–4 most probably show lower activities as they are in a suboptimal position for optimal force output (Siemienski, 1992). The activation pattern moreover reflects observations made for the spatial composition in higher insects. In Mantodea (Wipfler et al., 2012) and Neuroptera (Beutel et al., 2010), 0md1 shows a division into distinct bundles, and even in Odonata other than the one studied here, this muscle splits into several distinct bundles (Blanke et al., 2013c). Given our data, these divisions most probably reflect a development towards optimization of fibre quantity and spatial configuration, i.e. the use of less muscle mass to generate similar overall force outputs. Functional requirements of muscle organization may therefore play a crucial role and the phylogenetic value of different spatial muscle configurations of 0md1 (such as multiple attachments at the head capsule) is probably questionable. However, we cannot rule out that other effects such as fibre density optimization, fibre combination, properties of surrounding tissues or passive forces of joints might influence muscle configuration as well. For example, different muscle fibre-type combinations were reported for several ant species (Paul, 2001), and tissue properties in insects seem to be species and body part dependent, varying sometimes by several orders of magnitude (Hillerton, 1980; Hillerton et al., 1982; Vincent, 2002; Vincent and Wegst, 2004). Compared with musculoskeletal research in vertebrates, knowledge of insect muscle characteristics is only fragmentary and needs to be studied on a systematic level by investigating a range of species from different orders. Influences of joint geometries have up to now been impossible to model because of the small size of insect joints (~200 µm diameter for the ball-and-socket joint in *Sympetrum*); however, µCT methods will allow modelling of different joint geometries in insects in the near future.

The *in vivo* measurement of muscle parameters in insects has been done for model insects like *Carausius morosus* in order to study patterns of neuronal control, muscle activation and among-animal variation of muscle activation (Blümel et al., 2012a,b,c). Comparable *in vivo* measurements have not been done for insect heads so far because of the difficulty of assessing motor neurons and the whole range of muscle fibres and fibre types. So far, only comparably simple unipinnate muscles have been assessed experimentally (Blümel et al., 2012a,b,c) and the results suggest that large animal-to-animal variations in muscle parameters can occur for the measured muscle groups, which might affect force predictions of single muscles. In contrast, MDA case studies investigating simulated bite force against measured values show that muscle geometry and force orientation as well as realistic muscle wrapping have the highest influence on the accuracy of MDA models (Curtis et al., 2010a; Gröning et al., 2013). Regarding initial muscle activation, it was demonstrated that this does not depend critically on muscle model parameters (van Bolhuis and Gielen, 1999) but that activation is most probably a function of a stereotypical neuronal control pattern.

A potential avenue for validation of muscle activation patterns in millimetre-sized insects would be time-resolved µCT investigations of the internal anatomy (Schmitt et al., 2014; Walker et al., 2014). However, current image resolutions are too low to accurately model muscle geometries and obtain force–length curves and variations in cross-sectional areas.

Although it was shown that muscle model parameters do vary even between single individuals, our setup provides a useful toolbox for assessing general muscle activation patterns in extremely small specimens with complicated muscle geometries, where direct measurements are currently impossible. Information about muscle activation and force output is an invaluable basis for future studies on the head mechanics of insects. It will allow the study of optimization patterns across insects concerning structural design, material usage and more generally the evolution of insect mouthparts from a mechanical view.

Acknowledgements

We thank Christof Sonderegger of Kistler Instrumente AG for kindly providing the force sensor. We furthermore thank Jürgen Geiermann (German Sports University) who designed and constructed the fixation device. Susanne Duengelhoef, Björn M. von Reumont and Karen Meusemann are thanked for assistance during the SR-µCT experiments. Felix Beckmann and Fabian Wilde [both Helmholtz-Zentrum Geesthacht (HZG)/Deutsches Elektronen-Synchrotron DESY] provided excellent support at the synchrotron facilities. The useful discussions with Bernhard Misof and Benjamin Wipfler during the preparation of the manuscript are gratefully acknowledged.

Competing interests

The authors declare no competing or financial interests.

Author contributions

A.B., S.D. and W.P. designed the study; S.D. programmed the AnyBody Modeling System™ model; A.B. did the SR-µCT experiments and the segmentation and worked out the analysis pipeline together with S.D.; S.D., J.F. and A.B. did the force measurements. All authors wrote, read and approved the final version of the manuscript.

Funding

The financial support of the Deutsches Elektronen-Synchrotron (DESY: I-20120065) to perform synchrotron experiments is gratefully acknowledged. A.B. was financed by a research fellowship of the Deutsche Forschungsgemeinschaft (DFG: BL 1355/1-1). S.D. received funding from a graduate fellowship of the German Sports University (DSHS).

Supplementary information

Supplementary information available online at
http://jeb.biologists.org/lookup/suppl/doi:10.1242/jeb.132399/-/DC1

References

Bässler, U. (1988). Functional principles of pattern generation for walking movements of stick insect forelegs: the role of the femoral chordotonal organ afferences. *J. Exp. Biol.* **136**, 125-147.

Bates, K. T. and Falkingham, P. L. (2012). Estimating maximum bite performance in *Tyrannosaurus rex* using multi-body dynamics. *Biol. Lett.* **8**, 660-664.

Beckmann, F., Herzen, J., Haibel, A., Müller, B. and Schreyer, A. (2008). High density resolution in synchrotron-radiation-based attenuation-contrast microtomography. *Proc. SPIE* **7078**, 70781D-70781D–13.

Betz, O., Wegst, U., Weide, D., Heethoff, M., Helfen, L., Lee, W.-K. and Cloetens, P. (2007). Imaging applications of synchrotron X-ray phase-contrast microtomography in biological morphology and biomaterials science. I. General aspects of the technique and its advantages in the analysis of millimetre-sized arthropod structure. *J. Microsc.* **227**, 51-71.

Beutel, R. G. and Gorb, S. N. (2006). A revised interpretation of the evolution of attachment structures in Hexapoda with special emphasis on Mantophasmatodea. *Arthropod Syst. Phylogeny* **64**, 3-25.

Beutel, R. G., Zimmermann, D., Krauß, M., Randolf, S. and Wipfler, B. (2010). Head morphology of *Osmylus fulvicephalus* (Osmylidae, Neuroptera) and its phylogenetic implications. *Org. Divers. Evol.* **10**, 311-329.

Beutel, R. G., Friedrich, F., Ge, S. Q. and Yang, X. K. (2013). *Insect Morphology and Phylogeny*. Berlin: De Gruyter.

Bitsch, J. (1963). Morphologie céphalique des machilides (Insecta Thysaunura). *Ann. Sci. Nat. Zool.* **12**, 585-706.

Blaney, W. M. and Chapman, R. F. (1970). The functions of the maxillary palps of Acrididae (Orthoptera). *Entomol. Exp. Appl.* **13**, 363-376.

Blanke, A., Wipfler, B., Letsch, H., Koch, M., Beckmann, F., Beutel, R. and Misof, B. (2012). Revival of Palaeoptera head characters support a monophyletic origin of Odonata and Ephemeroptera (Insecta). *Cladistics* **28**, 560-581.

Blanke, A., Beckmann, F. and Misof, B. (2013a). The head anatomy of *Epiophlebia superstes* (Odonata: Epiophlebiidae). *Org. Divers. Evol.* **13**, 55-66.

Blanke, A., Greve, C., Wipfler, B., Beutel, R. G., Holland, B. R. and Misof, B. (2013b). The identification of concerted convergence in insect heads corroborates Palaeoptera. *Syst. Biol.* **62**, 250-263.

Blanke, A., Greve, C., Mokso, R., Beckmann, F. and Misof, B. (2013c). An updated phylogeny of Anisoptera including formal convergence analysis of morphological characters. *Syst. Entomol.* **38**, 474-490.

Blanke, A., Koch, M., Wipfler, B., Wilde, F. and Misof, B. (2014). Head morphology of *Tricholepidion gertschi* indicates monophyletic Zygentoma. *Front. Zool.* **11**, 16.

Blanke, A., Machida, R., Szucsich, N. U., Wilde, F. and Misof, B. (2015). Mandibles with two joints evolved much earlier in the history of insects: dicondyly is a synapomorphy of bristletails, silverfish and winged insects. *Syst. Entomol.* **40**, 357-364.

Blümel, M., Hooper, S. L., Guschlbauerc, C., White, W. E. and Büschges, A. (2012a). Determining all parameters necessary to build Hill-type muscle models from experiments on single muscles. *Biol. Cybern.* **106**, 543-558.

Blümel, M., Guschlbauer, C., Daun-Gruhn, S., Hooper, S. L. and Büschges, A. (2012b). Hill-type muscle model parameters determined from experiments on single muscles show large animal-to-animal variation. *Biol. Cybern.* **106**, 559-571.

Blümel, M., Guschlbauer, C., Hooper, S. L. and Büschges, A. (2012c). Using individual-muscle specific instead of across-muscle mean data halves muscle simulation error. *Biol. Cybern.* **106**, 573-585.

Brauckmann, C. and Zessin, W. (1989). Neue Meganeuridae aus dem Namurium von Hagen-Vorhalle (BRD) und die Phylogenie der Meganisoptera (Insecta, Odonata). *Dtsch. Entomol. Z.* **36**, 177-215.

Büschges, A., Akay, T., Gabriel, J. P. and Schmidt, J. (2008). Organizing network action for locomotion: insights from studying insect walking. *Brain Res. Rev.* **57**, 162-171.

Crowninshield, R. D. and Brand, R. A. (1981). A physiologically based criterion of muscle force prediction in locomotion. *J. Biomech.* **14**, 793-801.

Curtis, N., Jones, M. E. H., Evans, S. E., Shi, J., O'Higgins, P. and Fagan, M. J. (2010a). Predicting muscle activation patterns from motion and anatomy: modelling the skull of *Sphenodon* (Diapsida: Rhynchocephalia). *J. R. Soc. Interface* **7**, 153-160.

Curtis, N., Jones, M. E. H., Lappin, A. K., O'Higgins, P., Evans, S. E. and Fagan, M. J. (2010b). Comparison between in vivo and theoretical bite performance: using multi-body modelling to predict muscle and bite forces in a reptile skull. *J. Biomech.* **43**, 2804-2809.

Damsgaard, M., Rasmussen, J., Christensen, S. T., Surma, E. and de Zee, M. (2006). Analysis of musculoskeletal systems in the AnyBody Modeling System. *Simul. Model. Pract. Theory* **14**, 1100-1111.

Duprey, S., Savonnet, L., Black, N. and Wang, X. (2015). Muscle force prediction: can we rely on musculoskeletal model estimations? A case study on push force exertions with the upper limb. *Comput. Methods Biomech. Biomed. Engin.* **18** Suppl. 1, 1934-1935.

Evans, M. E. G. (1964). V.—A comparative account of the feeding methods of the beetles *Nebria brevicollis* (F.) (Carabidæ) and *Philonthus decorus* (Grav.) (Staphylinidæ). *Earth Environ. Sci. Trans. R. Soc. Edinb.* **66**, 91-109.

Forsythe, T. G. (1982). Feeding mechanisms of certain ground beetles (Coleoptera: Carabidae). *Coleopt. Bull.* **36**, 26-73.

Forsythe, T. G. (1983). Mouthparts and feeding of certain ground beetles (Coleoptera: Carabidae). *Zool. J. Linn. Soc.* **79**, 319-376.

Goyens, J., Dirckx, J., Dierick, M., Van Hoorebeke, L. and Aerts, P. (2014). Biomechanical determinants of bite force dimorphism in *Cyclommatus metallifer* stag beetles. *J. Exp. Biol.* **217**, 1065-1071.

Grimaldi, D. and Engel, M. S. (2005). *Evolution of the Insects*. Cambridge: Cambridge University Press.

Gronenberg, W. (1995). The fast mandible strike in the trap-jaw ant *Odontomachus*. *J. Comp. Physiol. A* **176**, 399-408.

Gronenberg, W., Paul, J., Just, S. and Hölldobler, B. (1997). Mandible muscle fibers in ants: fast or powerful?. *Cell Tissue Res.* **289**, 347-361.

Gröning, F., Jones, M. E. H., Curtis, N., Herrel, A., O'Higgins, P., Evans, S. E. and Fagan, M. J. (2013). The importance of accurate muscle modelling for biomechanical analyses: a case study with a lizard skull. *J. R. Soc. Interface* **10**, 20130216.

Hill, A. V. (1938). The heat of shortening and the dynamic constants of muscle. *Proc. R. Soc. Lond. B Biol. Sci.* **126**, 136-195.

Hillerton, J. E. (1980). The hardness of locust incisors. *Symp. Soc. Exp. Biol.* **34**, 483-484.

Hillerton, J. E., Reynolds, S. E. and Vincent, J. F. V. (1982). On the indentation hardness of insect cuticle. *J. Exp. Biol.* **96**, 45-52.

Hubel, T. Y. and Usherwood, J. R. (2015). Children and adults minimise activated muscle volume by selecting gait parameters that balance gross mechanical power and work demands. *J. Exp. Biol.* **218**, 2830-2839.

Julian, F. J. (1969). Activation in a skeletal muscle contraction model with a modification for insect fibrillar muscle. *Biophys. J.* **9**, 547-570.

Kubo, K., Kawakami, Y. and Fukunaga, T. (1999). Influence of elastic properties of tendon structures on jump performance in humans. *J. Appl. Physiol.* **87**, 2090-2096.

Misof, B., Liu, S., Meusemann, K., Peters, R. S., Donath, A., Mayer, C., Frandsen, P. B., Ware, J., Flouri, T., Beutel, R. G. et al. (2014). Phylogenomics resolves the timing and pattern of insect evolution. *Science* **346**, 763-767.

Moazen, M., Curtis, N., Evans, S. E., O'Higgins, P. and Fagan, M. J. (2008). Rigid-body analysis of a lizard skull: modelling the skull of *Uromastyx hardwickii*. *J. Biomech.* **41**, 1274-1280.

Ogden, T. H. and Whiting, M. F. (2003). The problem with "the Paleoptera Problem": sense and sensitivity. *Cladistics* **19**, 432-442.

Pandy, M. G. (2001). Computer modeling and simulation of human movement. *Annu. Rev. Biomed. Eng.* **3**, 245-273.

Pass, G. (2000). Accessory pulsatile organs: evolutionary innovations in insects. *Annu. Rev. Entomol.* **45**, 495-518.

Pass, G. (2006). Phylogenetic relationships of the orders of Hexapoda: contributions from the circulatory organs for a morphological data matrix. *Arthropod Syst. Phylogeny* **64**, 165-203.

Paul, J. (2001). Mandible movements in ants. *Comp. Biochem. Physiol. A Mol. Integr. Physiol.* **131**, 7-20.

Paul, J. and Gronenberg, W. (1999). Optimizing force and velocity: mandible muscle fibre attachments in ants. *J. Exp. Biol.* **202**, 797-808.

Paul, J. and Gronenberg, W. (2002). Motor control of the mandible closer muscle in ants. *J. Insect Physiol.* **48**, 255-267.

Popham, E. J. (1959). The anatomy in relation to feeding habits of *Forficula auricularia* L. and Other Dermaptera. *Proc. Zool. Soc. Lond.* **133**, 251-300.

Rasmussen, J., Damsgaard, M. and Voigt, M. (2001). Muscle recruitment by the min/max criterion — a comparative numerical study. *J. Biomech.* **34**, 409-415.

Romeis, B. (1989). *Mikroskopische Technik*. München: Urban & Schwarzenberg.

Schmitt, C., Rack, A. and Betz, O. (2014). Analyses of the mouthpart kinematics in *Periplaneta americana* (Blattodea, Blattidae) by using Synchrotron-based X-ray cineradiography. *J. Exp. Biol.* **217**, 3095-3107.

Siemienski, A. (1992). Soft saturation, an idea for load sharing between muscles. Application to the study of human locomotion. In (A. Cappozzo, M. Marchetti and V. Tosi), Proceedings of the Symposium "Biolocomotion: a Century of Research Using Moving Pictures". *Promograph Rome Italy* 293-303.

Spagna, J. C., Vakis, A. I., Schmidt, C. A., Patek, S. N., Zhang, X., Tsutsui, N. D. and Suarez, A. V. (2008). Phylogeny, scaling, and the generation of extreme forces in trap-jaw ants. *J. Exp. Biol.* **211**, 2358-2368.

Staniczek, A. H. (2000). The mandible of silverfish (Insecta: Zygentoma) and mayflies (Ephemeroptera): its morphology and phylogenetic significance. *Zool. Anz.* **239**, 147-178.

Staniczek, A. H. (2001). Der Larvenkopf von *Oniscigaster wakefieldi* McLachlan, 1873 (Insecta: Ephemeroptera: Oniscigastridae). Ein Beitrag zur vergleichenden Anatomie und Phylogenie der Eintagsfliegen. PhD thesis, Eberhard-Karls-Universität Tübingen.

Terry, M. D. and Whiting, M. F. (2005). Mantophasmatodea and phylogeny of the lower neopterous insects. *Cladistics* **21**, 240-257.

Journal of Experimental Biology

Thelen, D. G. (2003). Adjustment of muscle mechanics model parameters to simulate dynamic contractions in older adults. *J. Biomech. Eng.* **125**, 70-77.
van Bolhuis, B. M. and Gielen, C. C. A. M. (1999). A comparison of models explaining muscle activation patterns for isometric contractions. *Biol. Cybern.* **81**, 249-261.
Vincent, J. F. V. (2002). Arthropod cuticle: a natural composite shell system. *Compos. Part Appl. Sci. Manuf.* **33**, 1311-1315.
Vincent, J. F. V. and Wegst, U. G. K. (2004). Design and mechanical properties of insect cuticle. *Arthropod Struct. Dev.* **33**, 187-199.
von Kéler, S. (1963). *Entomologisches Wörterbuch mit Besonderer Berücksichtigung der Morphologischen Terminologie*. Berlin: Akademie-Verlag.
Walker, S. M., Schwyn, D. A., Mokso, R., Wicklein, M., Müller, T., Doube, M., Stampanoni, M., Krapp, H. G. and Taylor, G. K. (2014). In vivo time-resolved microtomography reveals the mechanics of the blowfly flight motor. *PLoS Biol.* **12**, e1001823.
Watson, P. J., Gröning, F., Curtis, N., Fitton, L. C., Herrel, A., McCormack, S. W. and Fagan, M. J. (2014). Masticatory biomechanics in the rabbit: a multi-body dynamics analysis. *J. R. Soc. Interface* **11**, 20140564.
Wehner, T., Wolfram, U., Henzler, T., Niemeyer, F., Claes, L. and Simon, U. (2010). Internal forces and moments in the femur of the rat during gait. *J. Biomech.* **43**, 2473-2479.
Weihmann, T., Reinhardt, L., Weißing, K., Siebert, T. and Wipfler, B. (2015). Fast and powerful: biomechanics and bite forces of the mandibles in the American Cockroach *Periplaneta americana*. *PLoS ONE* **10**, e0141226.
Wheater, C. P. and Evans, M. E. G. (1989). The mandibular forces and pressures of some predacious Coleoptera. *J. Insect Physiol.* **35**, 815-820.
Wheeler, W. C., Whiting, M., Wheeler, Q. D. and Carpenter, J. M. (2001). The phylogeny of the extant hexapod orders. *Cladistics* **17**, 113-169.
Willkommen, J. and Hörnschemeyer, T. (2007). The homology of wing base sclerites and flight muscles in Ephemeroptera and Neoptera and the morphology of the pterothorax of *Habroleptoides confusa* (Insecta: Ephemeroptera: Leptophlebiidae). *Arthropod Struct. Dev.* **36**, 253-269.
Wipfler, B., Machida, R., Müller, B. and Beutel, R. G. (2011). On the head morphology of Grylloblattodea (Insecta) and the systematic position of the order, with a new nomenclature for the head muscles of Dicondylia. *Syst. Entomol.* **36**, 241-266.
Wipfler, B., Wieland, F., DeCarlo, F. and Hörnschemeyer, T. (2012). Cephalic morphology of *Hymenopus coronatus* (Insecta: Mantodea) and its phylogenetic implications. *Arthropod Struct. Dev.* **41**, 87-100.
Yushkevich, P. A., Piven, J., Hazlett, H. C., Smith, R. G., Ho, S., Gee, J. C. and Gerig, G. (2006). User-guided 3D active contour segmentation of anatomical structures: significantly improved efficiency and reliability. *NeuroImage* **31**, 1116-1128.
Zajac, F. E. (1989). Muscle and tendon: properties, models, scaling, and application to biomechanics and motor control. *Crit. Rev. Biomed. Eng.* **17**, 359-411.
Zatsiorsky, V. (2002). *Kinetics of Human Motion*. Champaign, IL: Human Kinetics Publishers.

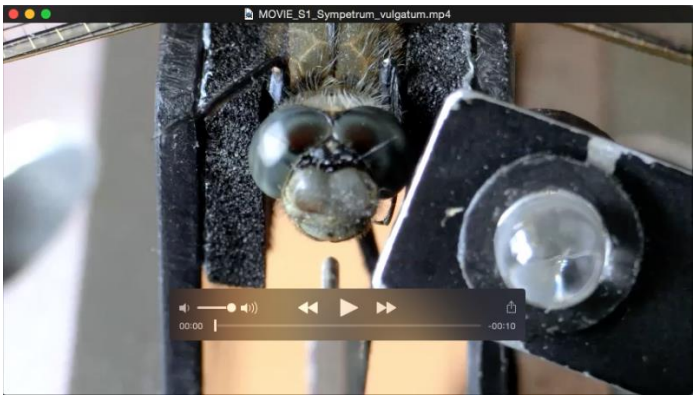

Movie 1. Film sequence showing the mandible movement of a living dragonfly during biting.

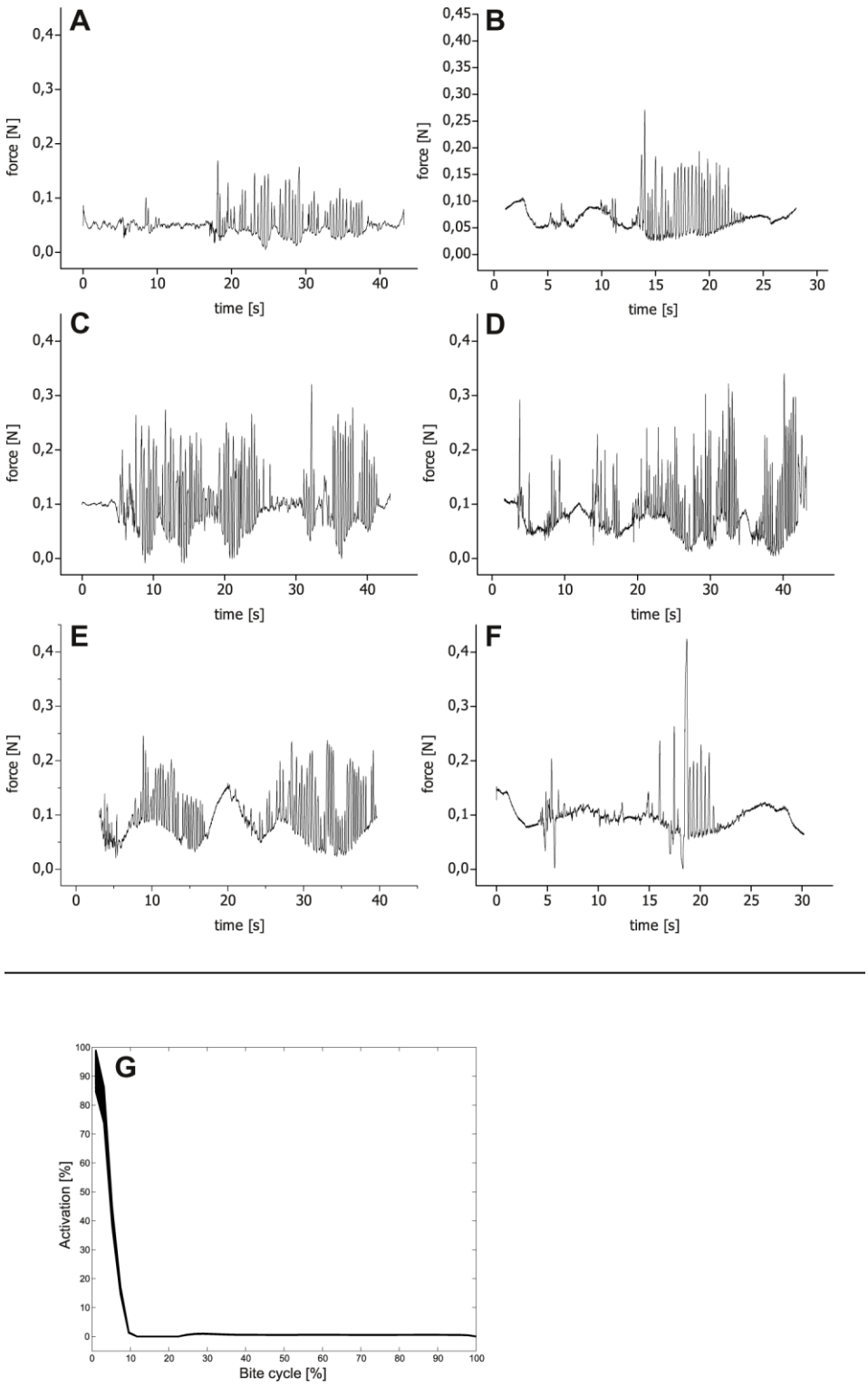

Fig. S1. (A-F) Bite cycles measured for *Sympetrum vulgatum*. Signal is bandpass filtered [0.1, 50 Hz]. (G) Activation of the mandibular abductor M. craniomandibularis externus posterior (0md3). Activation of this muscle is the same for all biting scenarios.